COMPUTER CLASSIFICATION OF RESERVOIR SANDSTONES

by

R. M. Haralick

K. Shanmugam

Department of Electrical Engineering and
The University of Kansas Center for Research, Inc.
Lawrence, Kansas 66044

Abstract -- A procedure is developed to extract numerical features which characterize the pore structure of reservoir rocks. The procedure is based on a set of descriptors which give a statistical description of porous media. These features are evaluated from digitized photomicrographs of reservoir rocks and they characterize the rock grain structure in terms of (1) the linear dependency of grey tones in the photomicrograph image, (2) the degree of "homogeneity" of the image and (3) the angular variations of the image grey tone dependencies. On the basis of these textural features, a simple identification rule using piecewise linear discriminant functions is developed for categorizing the photomicrograph images. The procedure was applied to a set of 243 distinct images comprising 6 distinct rock categories. The coefficients of the discriminant functions were obtained using 143 training samples. The remaining (100) samples were then processed, each sample being assigned to one of 6 possible sandstone categories. Eighty-nine per cent of the test samples were correctly identified.

Introduction

In recent years, high speed digital computers have been widely used in the implementation of two-dimensional image processing and classification techniques. These digital techniques are currently used in a variety of applications in the fields of biomedical image processing, remotely sensed radar and multispectral scanner imagery analysis and other fields (Hall et al. [1], Rosenfeld [2], Andrews [3] and NASA [4] and [5]). In this paper we present a procedure for automatic analysis and identification of digitized photomicrographs of the pore structure of reservoir rocks.

The analysis of the pore structure of the reservoir rock is important to geologists and petroleum engineers, who are interested in obtaining a series of numerical descriptors or features which statistically describe porous materials. If these features are valid, they may eventually be used for the prediction of the physical properties of porous media including porosity, specific permeability and formation factor which are important components in production studies.

In recent years, several investigators had attempted to evaluate and numerically characterize porous media. Pereze-Rosales [6,7], Davis [8], Preston, Green and Davis [9], Preston and Davis [10] have developed techniques to obtain features of photomicrographs of porous media to describe their characteristics.

Preston, Green and Davis [9] characterize the pore structure of rocks using values of the discrete power spectrum of specially prepared thin sections from reservoir sandstones. Their work is an extension of an earlier suggestion by Fara and Scheidegger [11] who stated that pore-grain geometries could be characterized by Fourier series fitted to a special function obtained from photomicrographs of sections through the rock. Preston, Green and Davis conclude that power spectra are statistically appropriate numerical descriptors of pore-grain geometry of porous media. In our present work, we use the textural features of the digitized photomicrographs of porous rocks to characterize and identify these photomicrograph images.

Manuscript received September 11, 1972, revised January 30, 1973.

An overview of the automatic image analysis scheme is shown in Figure 1.

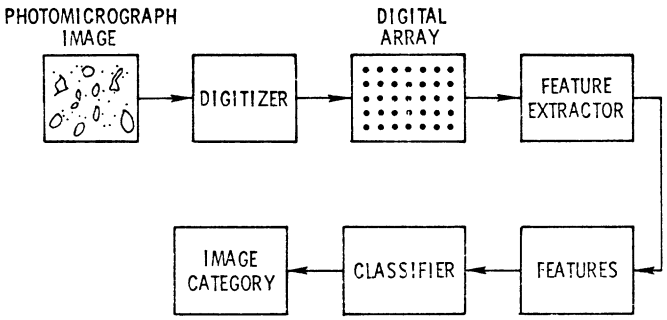

Figure 1. Block Diagram of Automatic Image Analysis Scheme.

The photomicrograph of the rock sample to be analyzed is first digitized to yield a digital image which is stored as a two dimensional array. Each entry in the digital array represents the average grey level of the corresponding cell of the original image. The digital image contains a large amount of redundant information. While this large amount of information in imagery data may be necessary for preserving the visual quality of the image, all of this information in general is not necessary for discriminating between various image categories. For discrimination purposes it may be sufficient to consider a small set of image descriptors (i.e., features).

Feature Extraction Procedure

Other than some work with the Fourier, Hadamard Transforms and the autocorrelation function, there exists little or no theory to aid in establishing what the textural features should consist of. Rather, the feature extraction operation is determined intuitively, rationalized heuristically and later justified pragmatically and empirically. For automatic analysis of photomicrograph, and other imagery we have developed a procedure to extract features from the spatial grey tone dependence matrix which is computed for each photomicrograph image.

Spatial Grey Tone Dependence Matrix

Let $L_x = \{1,2,\ldots,N_x\}$ and $L_y = \{1,2,\ldots,N_y\}$ be the x and y spatial domains and $L_y \times L_x$ be the set of resolution cells. Let $G = \{0,1,\ldots,N_g\}$ be the set of possible grey tones. Then a digital image I is a function which assigns* some grey tone to each and every resolution cell; $I: L_y \times L_x \rightarrow G$.

An essential component of our conceptual framework of texture is a matrix or more precisely, four closely related matrices from which all texture-context features are derived. These matrices are termed angular nearest neighbor grey tone spatial dependence matrices.

*The spatial domain $L_y \times L_x$ consists of ordered pairs whose components are row and column respectively. This convention conforms with the usual two subscript row-column designation used in FORTRAN.

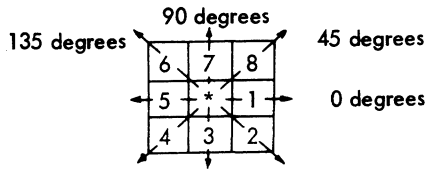

Figure 2. Distance 1 neighbors. Resolution cells number 1 and 5 are the 0-degree (horizontal) nearest neighbors to resolution cell '*', resolution cells numbers 2 and 6 are the 135-degree nearest neighbors, resolution cells 4 and 8 are the 45-degree nearest neighbors to '*'. (Note that this information is purely spatial, and has nothing to do with grey tone values).

We assume that the texture-context information in an image I is contained in the over-all or "average" spatial relationship which the grey tones in image I have to one another. More specifically, we shall assume that this texture-context information is adequately specified by the matrix of relative frequencies P_{ij} with which two neighboring resolution cells separated by distance d occur on the image, one with grey tone i and the other with grey tone j (see Figure 2). Such matrices of spatial grey tone dependence frequencies are a function of the angular relationship between the neighboring resolution cells as well as a function of the distance between them. The set of all horizontal neighboring resolution cells separated by distance 1 along with the image grey tones will be used to calculate a distance 1 horizontal spatial grey tone dependence matrix. Formally, for angles quantized to 45° intervals the unnormalized frequencies are defined by:

$$P(i,j,d,0^\circ) = \#\{((k,l),(m,n)) \in (L_y \times L_x) \times (L_y \times L_x) \mid k-m=0,\ |l-n|=d,\ I(k,l)=i,\ I(m,n)=j\}$$

$$P(i,j,d,45^\circ) = \#\{((k,l),(m,n)) \in (L_y \times L_x) \times (L_y \times L_x) \mid (k-m=d,\ l-n=-d) \text{ or } (k-m=-d,\ l-n=d),\ I(k,l)=i,\ I(m,n)=j\}$$

$$P(i,j,d,90^\circ) = \#\{((k,l),(m,n)) \in (L_y \times L_x) \times (L_y \times L_x) \mid |k-m|=d,\ l-n=0,\ I(k,l)=i,\ I(m,n)=j\}$$

$$P(i,j,d,135^\circ) = \#\{((k,l),(m,n)) \in (L_y \times L_x) \times (L_y \times L_x) \mid (k-m=d,\ l-n=d) \text{ or } (k-m=-d,\ l-n=-d),\ I(k,l)=i,\ I(m,n)=j\}$$

Note that these matrices are symmetric; P(i,j; d,a) = P(j,i; d,a). The distance metric ρ implicit in the above equations is the l_∞ norm and can be explicitly defined by [12]:

$$\rho((k,l),(m,n)) = \left\{|k-m|^\infty + |l-n|^\infty\right\}^{\frac{1}{\infty}},$$

which reduces to

$$\rho((k,l),(m,n)) = \max\{|k-m|, |l-n|\}.$$

Consider Figure 3-a, which represents a 4 x 4 image with four grey tones, ranging from 0 to 3. Figure 3-b shows the general form of any grey tone spatial dependence matrix. For example, the element in the (2,1) position of the distance 1 horizontal P_H matrix is the total number of times two grey tones of value 2 and 1 occurred horizontally adjacent to each other. To determine this number, we count the number of pairs of resolution cells in R_H such that the first resolution cell of the pair has grey tone 2 and the second resolution cell of the pair has grey tone 1. In Figures 3-c through 3-f we calculate all four distance 1 grey tone spatial dependence matrices.

0	0	1	1
0	0	1	1
0	2	2	2
2	2	3	3

Figure 3-a.

Grey Tone	0	1	2	3
0	#(0,0)	#(0,1)	#(0,2)	#(0,3)
1	#(1,0)	#(1,1)	#(1,2)	#(1,3)
2	#(2,0)	#(2,1)	#(2,2)	#(2,3)
3	#(3,0)	#(3,1)	#(3,2)	#(3,3)

Figure 3-b. This shows the general form of any grey tone spatial dependence matrix for an image with integer grey tone values 0 to 3. #(i,j) stands for number of times grey tones i and j have been neighbors.

0° $P_H = \begin{pmatrix} 4 & 2 & 1 & 0 \\ 2 & 4 & 0 & 0 \\ 1 & 0 & 6 & 1 \\ 0 & 0 & 1 & 2 \end{pmatrix}$

Figure 3-c.

90° $P_V = \begin{pmatrix} 6 & 0 & 2 & 0 \\ 0 & 4 & 2 & 0 \\ 2 & 2 & 2 & 2 \\ 0 & 0 & 2 & 0 \end{pmatrix}$

Figure 3-d.

135° $P_{LD} = \begin{pmatrix} 2 & 1 & 3 & 0 \\ 1 & 2 & 1 & 0 \\ 3 & 1 & 0 & 2 \\ 0 & 0 & 2 & 0 \end{pmatrix}$

Figure 3-e.

45° $P_{RD} = \begin{pmatrix} 4 & 1 & 0 & 0 \\ 1 & 2 & 2 & 0 \\ 0 & 2 & 4 & 1 \\ 0 & 0 & 1 & 0 \end{pmatrix}$

Figure 3-f.

The appropriate frequency normalization for these matrices can be easily computed.

Textural Features and Their Significance

From each of these four grey tone dependence matrices we extract four texture context features of the following forms:

$$\sum_{a=1}^{N_g} \sum_{b=1}^{N_g} \left[\frac{P(a,b)}{\#R}\right]^2 \quad \text{, the angular second moment (ASM);}$$

$$\frac{COV}{VAR} = \frac{\sum_{a=1}^{N_g} \sum_{b=1}^{N_g} \frac{ab\,P(a,b)}{\#R} - \mu_a \mu_b}{\sigma_a \sigma_b} \quad \text{, the correlation between neighboring grey tones (COR);}$$

$$\mu_a = \left[\sum_{a=1}^{N_g} \sum_{b=1}^{N_g} \frac{a\,P(a,b)}{\#R}\right]$$

$$\mu_b = \left[\sum_{a=1}^{N_g} \sum_{b=1}^{N_g} \frac{b\,P(a,b)}{\#R}\right]$$

$$\sigma_a = \left[\sum_{a=1}^{N_g} \sum_{b=1}^{N_g} a^2 \frac{P(a,b)}{\#R} - \left(\sum_{a=1}^{N_g} \sum_{b=1}^{N_g} \frac{a\,P(a,b)}{\#R}\right)^2\right]^{1/2}$$

$$\sigma_b = \left[\sum_{a=1}^{N_g} \sum_{b=1}^{N_g} b^2 \frac{P(a,b)}{\#R} - \left(\sum_{a=1}^{N_g} \sum_{b=1}^{N_g} b\,\frac{P(a,b)}{\#R}\right)^2\right]^{1/2}$$

$$\sum_{a=1}^{N_g}\sum_{b=1}^{N_g}\left(\frac{P(a,b)}{\#R}\right)\log\left(\frac{\#R}{P(a,b)}\right)$$, the entropy (ENT);

$$\sum_{n=1-N_g}^{N_g-1} n^2\left[\sum_{\substack{a-b\\ a-b=n}}\frac{P(a,b)}{\#R}\right]^2$$, the contrast (CONT);

Note: $\#R$ is the number of neighboring resolution cells.

To explain the significance of these measures let us consider the kinds of values they assume on different types of photomicrograph images. Figure 4 shows two types of images and their textural feature values. The image of the Dexter sandstone has fewer dominant grey tones and fewer dominant grey tone transitions compared to the image of the Upper Muddy sandstone. Accordingly the P matrix for Dexter image will have fewer entries of larger magnitude and the P matrix for Upper Muddy sandstone image will have a large number of small entries. Hence the ASM feature, computed using the squared values of the entries in the P matrix, has a larger value for the Dexter image than for the Upper Muddy sandstone image. The entropy feature for the Dexter sandstone image has a lower value since the Upper Muddy sandstone matrix has more small values.

The grain structure for the Dexter sandstone appears to be packed more orderly compared to the grain structure of the Upper Muddy sandstone. The orderly packed grain structure of the Dexter sandstone leads to higher value for the (COR) correlation feature which gives an idea of the linear grey tone dependencies in the image.

The various features which we suggest are all functions of distance and angle. The angular dependencies present a special problem. Suppose image A has features a, b, c, d for angles 0°, 45°, 90° and 135° and image B is identical to A except that B is rotated 90° with respect to A. Then B will have features c, d, a, b for angles 0°, 45°, 90° and 135° respectively. Since the texture context of A is the same as the texture context of B, any decision rule using the angular features a, b, c, d must produce the same results for c, d, a, b or for that matter b, c, d, a (45° rotation) and d, a, b, c (135° rotation). To guarantee this, we do not use the angularly dependent features directly. Instead, we use two symmetric functions of a, b, c, d, their average and their range. These features can be represented in vector form $F = [f_1, f_2, \ldots, f_n]^T$, where $f_1, f_2, \ldots, f_n$ are the values of the features, T denotes the transpose.

The usefulness of these features for numerical characterization of the pore structure of reservoir rock can be analyzed by using these features to categorize the photomicrograph images. A high identification accuracy will indicate that these features adequately describe the pore grain geometry of reservoir rocks. Since the physical properties of rocks such as porosity are related to the grain structure of the rocks, these features may be used in a regression model to predict the physical properties of porous media including porosity, specific permeability and formation factor.

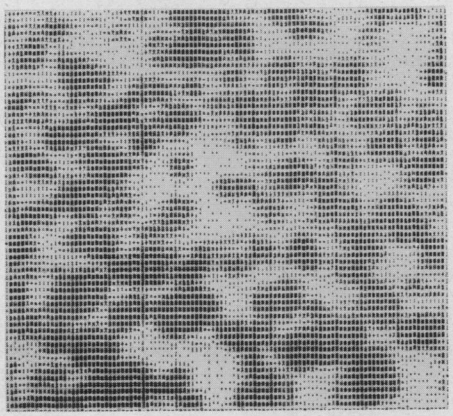

Digitized Photomicrograph of
a. Dexter Sandstone

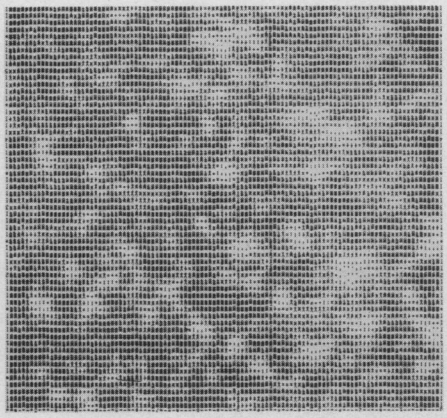

Digitized Photomicrograph of
b. Upper Muddy Sandstone

	ASM	COR	ENT	ASM	COR	ENT
0°	0.0182	0.8093	4.8091	0.0068	0.6532	5.1906
45°	0.0148	0.7098	4.9884	0.0054	0.4657	5.3536
90°	0.0212	0.8522	4.7133	0.0068	0.6463	5.1938
135°	0.0144	0.7031	5.0023	0.0053	0.4247	5.3740
Average	0.0171	0.7561	4.8782	0.0061	0.5449	5.2780

Figure 4. Textural Features of Two Different Photomicrograph Image Samples.

Identification Procedure

The problem of developing procedures for categorizing environmental units consists of the following:

With reference to Figure 5, the universe U consists of environmental units (for example rocks) $U_1, U_2, \ldots, U_T$ which belong to one of R possible categories $C_1, C_2, \ldots, C_R$ (different rock categories). Of the large number of environmental units present in the universe, we observe a smaller subset of units $U_1, U_2, \ldots, U_N$. Our observations consist of a set of measured values of n features $f_1, f_2, \ldots, f_n$ for each unit U sampled. Based on the information contained in the feature vectors $F_1, F_2, \ldots, F_N$, for which the categories of the environmental units which produce these measurements is known, we want to develop an algorithm to identify the categories of new units based on the measurements they produce.

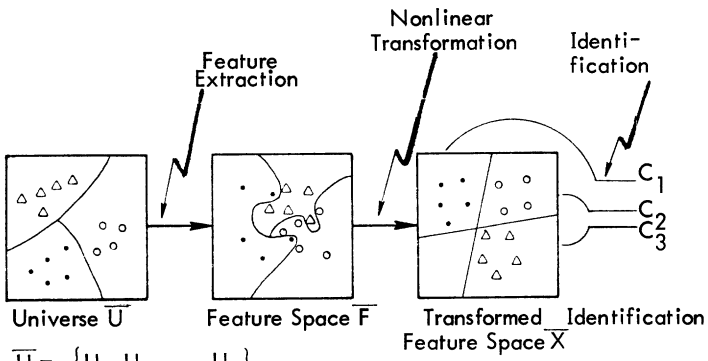

$\overline{U} = \{U_1, U_2, \ldots, U_T\}$

$\overline{F} = \{F_1, F_2, \ldots, F_T\}$; $F = [f_1\ f_2\ \ldots\ f_n]^T$

$\overline{X} = \{X_1, X_2, \ldots, X_T\}$; $X = [x_1 x_2\ \ldots\ x_m]^T$

The vectors F_i and X_i are usually referred to as the i^{th} feature vector and the i^{th} pattern vector respectively.

Figure 5. Identification Scheme.

The decision rule which assigns categories based on the values of features may be implemented in the feature space $\overline{F}$ by partitioning $\overline{F}$ into various regions and assigning categories to new units based on the regions to which their feature vectors belong. Efficient partitioning of the feature space may require complicated nonlinear decision boundaries (discriminant functions). Instead of deriving a decision rule in the feature space $\overline{F}$, we may transform the feature vectors into a new space $\overline{X}$ and implement a decision rule in the new space $\overline{X}$. By using appropriate nonlinear transformations, we may be able to implement nonlinear decision boundaries in $\overline{F}$ as linear decision boundaries in $\overline{X}$. Several procedures are available for deriving linear decision boundaries for partitioning $\overline{X}$ into various regions, based on the information contained in a set of sample patterns $X_1, X_2, \ldots, X_N$ whose categories are known.

Identification Algorithms

In a widely used algorithm (Fukunaga [13], Fu and Mendel [14], Miesel [15], the pattern space $\overline{X}$ is separated into a number of regions using a set of hyperplanes (decision boundaries) whose locations are determined by the sample patterns. Each region is dominated by sample patterns of a particular category. When a new pattern is presented for identification, it is assigned a category depending on the region in which it belongs. If the new pattern X is located in a region dominated by sample patterns of category C_j, then X is classified as coming from category C_j.

For the multicategory problem involving N_R categories, a total of $N_R(N_R-1)/2$ hyperplanes are used to partition the pattern space. These hyperplanes are defined by a set of weight vectors W_{ij} ($i = 1,2,\ldots,N_R$, $j = 1,2,\ldots,N_R$; $j > i$) which separates the sample patterns belonging to the i^{th} and j^{th} categories. A regression type algorithm given in Fukunaga (Chapter -4) was used to obtain the weight vectors. After the location of the hyperplanes are determined, the classification of new patterns is done as follows. For each category C_i, the number of hyperplanes, V_i, which give a positive response when the new pattern X is presented are determined using

$$V_i = \sum_{\substack{j=1 \\ j \neq i}}^{N_R} \frac{|W_{ij}^T Z| + W_{ij}^T Z}{2|W_{ij}^T Z|} \quad ; \quad i = 1,2,\ldots N_R$$

where Z is the augmented pattern vector obtained by adding a component of value 1 to X, i.e.,

$$Z = \begin{bmatrix} 1 \\ X \end{bmatrix}.$$

X is assigned to category C_j if

$$V_j = \max_i \{V_i\}$$

If there is a tie between categories C_m and C_n, then X is assigned to C_m if $W_{mn}^T Z \geq 0$ or to C_n if $W_{mn}^T Z < 0$. Several modifications of the linear discriminant function method and a multitude of other classification procedures may be found in the references cited.

Identification Experiments

Samples Used: The feature extraction and identification procedures were applied to a set of 243 photomicrograph images obtained from seven porous sandstone samples. The rock samples were impregnated with a special epoxide plastic that is very fluid and yet very hard when catalytically cured. A red dye was added to the plastic and the impregnated chips were used to make conventional thin sections which were then contact printed on to Kodalith film. Because this film is insensitive to red, it is exposed by light shining through the grains but not that shining through the red plastic filled pores. A high contrast pore-grain image is thus created on the film. Enlargements of films of the seven samples are shown in Figure 6. These were made at a magnification 3x directly from the images of the 35 mm film.

The geological description and the physical properties of the sandstone samples are presented in table 1. The Dexter sandstone samples used in our study were obtained from widely separated locations in Texas. An inspection of the Dexter images 6a, 6b, 6c and their physical properties reveals that the characteristics of the Dexter sample shown in 6b are quite different from the characteristics of samples 6a and 6c. Accordingly, the Dexter samples were treated as two distinct categories for identification experiments. The highly porous Dexter sample shown in Figure 6b was labeled as Dexter-H and the Dexter samples 6a and 6c with low porosity were labeled as Dexter-L. The two samples of St. Peter sandstones have identical characteristics and hence were treated as one category.

The high contrast film images were optically digitized, by measuring the optical transmission of the film at 8 μ spots spaced on a 24μ x 24μ grid across the film. The digital array was of size 1024 x 1024. Each of the 1024 x 1024 images were divided into 64 non-overlapping sections of size 128 x 128. Samples of 128 x 128 sections from the middle of each of the seven larger images were used for developing and testing the identification procedure. Thirty-six samples were taken from each of the images, except from the St. Peter image 6e and the Gaskel image 6g from which 33 and 30 samples respectively were taken.

TABLE I. Geological Description and Properties of Sandstone Samples

Figure	Formation	Location (Depth)	Average Porosity %	Average Permeability md.
6a	Dexter	Denton Co. Texas (outcrop)	17.30	21.50
6b	Dexter	Denton Co. Texas (outcrop)	26.20	8.0
6c	Dexter	Denton Co. Texas (outcrop)	17.90	20.70
6d	St. Peter	Redfield, Iowa (1,758')	19.23	987.00
6e.	St. Peter	Redfield, Iowa (1,758')	19.00	1,112.00
6f	Upper Muddy	Gas Drawfield Wyoming (7,366')	12.70	84.00
6g	Gaskel	Coalinga Nose Field California (7,500')	7.32	8.30

Before the textural features were extracted, the 128 x 128 arrays were compressed to 64 x 64 arrays by averaging 4 elements in non-overlapping 2 x 2 sections. The grey levels in the 64 x 64 array were normalized using equal probability quantization with 16 levels. This normalization eliminates the variations in the grey levels which might have resulted from variations in lighting, lens, film, developer and other processing variables.

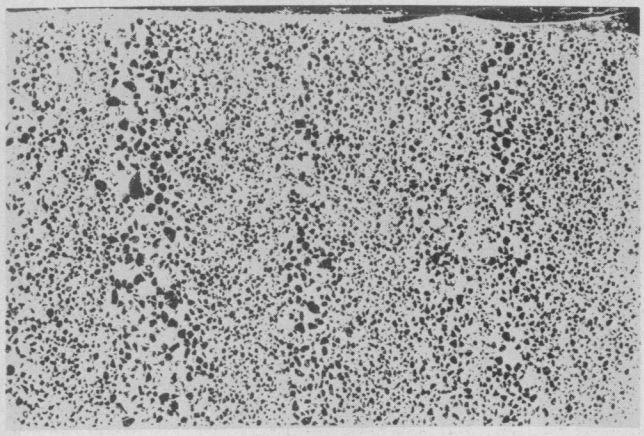

Figure 6a. Dexter sandstone, section P-1AV-01, courtesy of Professor Charles F. Dodge, API Project 91A, magnification 3x, File 1.

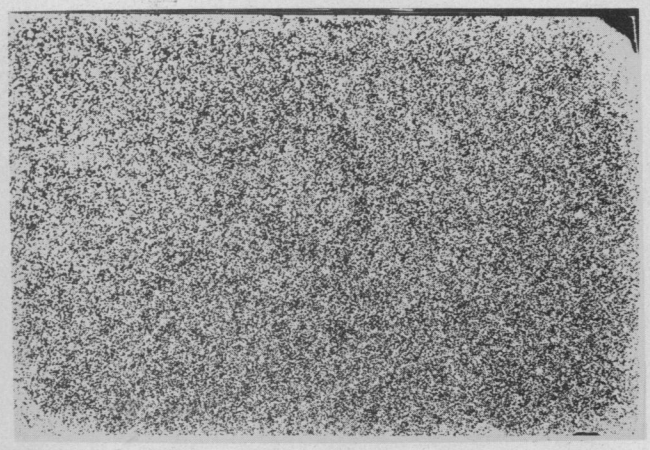

Figure 6b. Dexter sandstone, section T-1-R-83, courtesy of Professor Charles F. Dodge, API Project 91A, magnification 3x, File 2.

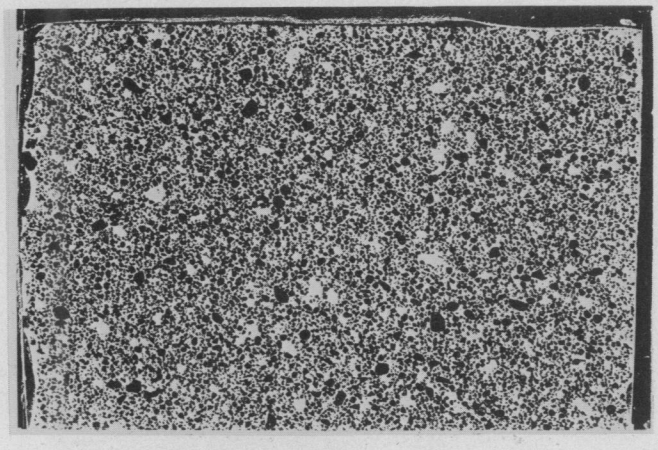

Figure 6c. Dexter sandstone, section T-1-R-30, courtesy of Professor Charles F. Dodge, API Project 91A, magnification 3x, File 3.

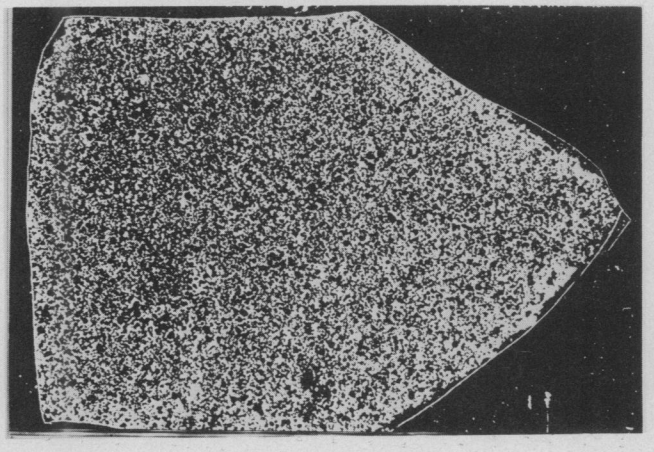

Figure 6d. Saint Peter sandstone, section C-S2, magnification 3x, File 4.

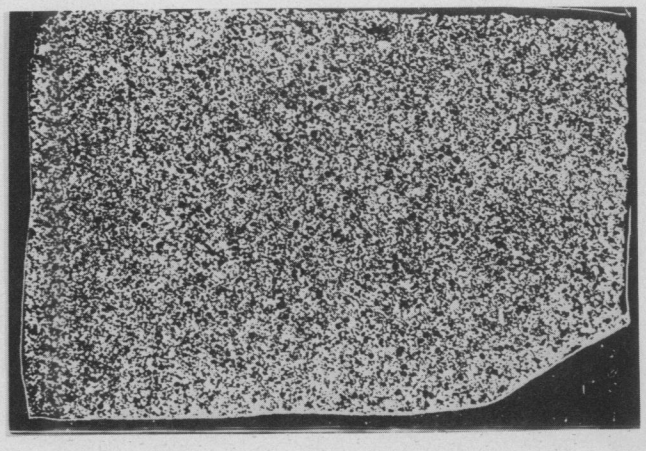

Figure 6e. Saint Peter sandstone, section C-S3, magnification 3x, File 5.

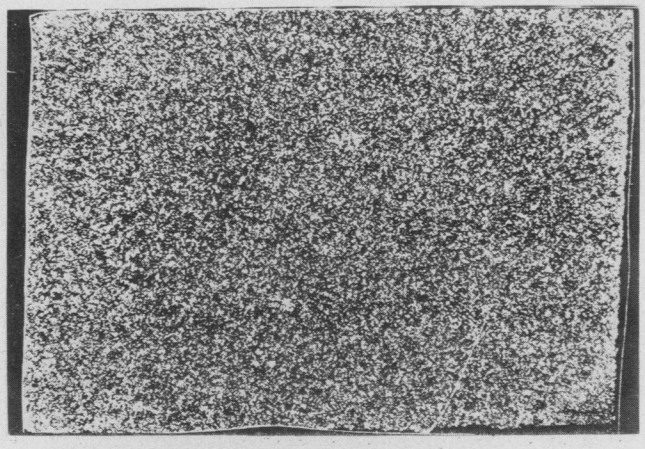

Figure 6f. Upper Muddy sandstone, section E-S8, magnification 3x, File 6.

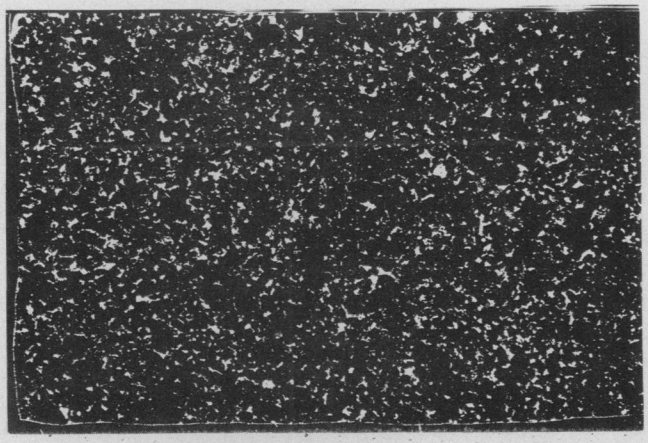

Figure 6g. Gaskel sandstone, section A-S4, magnification 3x, File 7.

Results of Identification Experiments

For each of the 243 image samples, the following set of 8 features were obtained:

ASM	average	(Distance 1)	f_1
	range		f_2
ENT	average	(Distance 1)	f_3
	range		f_4
COR	average	(Distance 1)	f_5
	range		f_6
CONT	average	(Distance 1)	f_7
	range		f_8

Along with the features $f_1, f_2, \ldots, f_8$, second degree Φ polynomials (Nilsson [16]) of the features (e.g. f_1^2, $f_1 f_2$), were also used in the identification algorithm.

The set of 243 samples was randomly divided into two groups. A group of 143 samples was used to develop the identification algorithm and the remaining 100 samples were used for testing the identification scheme. A total of 10 hyperplanes were used for separating the training patterns pairwise. Using a majority vote on these hyperplanes, each of the 100 test patterns were assigned to one of the five categories: Dexter L (low porosity), Dexter H (high porosity), St. Peter, Upper Muddy and Gaskel Sandstone. The results of classification are shown in table II and III.

Table II. Contingency table of true category versus assigned category. Variables used: f_1, f_2, f_3, f_4, f_5, f_6, f_7 and f_8. Identification accuracy = 89%.

		ASSIGNED CATEGORY					Total Samples Identified
		Dexter-L	Dexter-H	St. Peter	Upper Muddy	Gaskel	
TRUE CATEGORY	Dexter-L	29	0	1	0	0	30
	Dexter-H	0	15	0	0	0	15
	St. Peter	2	0	22	4	0	28
	Upper Muddy	0	0	4	11	0	15
	Gaskel	0	0	0	0	12	12
							100

Table III. Identification accuracy with polynomial discriminant functions.

Features	Variables used in Polynomial	Identification Accuracy on Test Samples
f_1, f_3, f_5	$f_1, f_3, f_5, f_1^2, f_3^2, f_5^2$ f_1f_3, f_1f_5, f_3f_5	86%
f_1, f_3, f_5, f_7	$f_1, f_3, f_5, f_7, f_1^2, f_3^2, f_5^2,$ $f_7^2, f_1f_3, f_1f_5, f_1f_7, f_3f_5,$ f_3f_7, f_5f_7	88%

The identification accuracy achieved with a linear discriminant function on the 8 features was 89 per cent on the test samples. Table I shows the details of the identification performance. The identification experiment was repeated with polynomial discriminant functions, achieving up to 88 per cent correct identification rate on the test samples. The classifier was also asked to identify the training samples which were used in deriving the discriminant functions. The identification accuracy on the training samples was 93 per cent for the linear discriminant function and, 91 per cent and 92 per cent repectively for the two nonlinear discriminant functions listed in Table III.

Most of the feature extraction and classification algorithms were programmed on a PDP-15 computer with 12K words of memory. These programs may be implemented on any medium sized general purpose digital computer. Complete details of the programs may be found in Haralick [17].

Discussion

A procedure has been presented to numerically characterize and identify photomicrographs of reservoir rocks. A set of 243 samples of digitized photomicrograph images were analyzed

automatically. Identification accuracy of 89 per cent was achieved when the training and testing of the classifier are done using different sets of images. When the training and testing were done on the same data set, 93 per cent accuracy was achieved. The high accuracy of classification indicates that the textural features are useful for describing the pore-grain geometry of natural porous materials. Since the physical properties of porous materials are a function of the pore grain geometry, it is our conjecture that the textural features may eventually be used in a regression model for predecting the physical properties of porous sandstones including porosity, specific permeability and formation factor which are important in production studies. It may be possible to increase the identification accuracy by using additional features (Haralick [17], Rosenfeld [18] and by using more powerful identification methods.

Acknowledgments

The authors wish to acknowledge the financial support provided by the U. S. Army Engineer Topographic Laboratory, under contract no. DAAK02-70-C-0388 through the Remote Sensing Laboratory for the textural feature extraction part. The authors wish to thank Professors Floyd Preston and John Davis for providing us with the core sample images and for their encouragement throughout the course of this work.

References

[1] Hall, E. L., et al., "A Survey of Preprocessing and Feature Extraction Techniques for Radiographic Images," IEEE Trans. on Computers, vol. 6-20, pp. 1032-1044, 1971.

[2] Rosenfeld, A., Picture Processing by Computer, Academic Press, New York, 1969.

[3] Andrews, H. C., Computer Techniques in Image Processing, Academic Press, New York, 1970.

[4] NASA Report, Third Annual Earth Resources Program Review, NASA MSC Report No. MSC 03742, December, 1970.

[5] NASA Report, Fourth Annual Earth Resources Program Review, NASA MSC Report No. MSC 05397, January, 1972.

[6] Pereze-Rosales, C., "Simultaneous Determination of Basic Geometric Characteristics of Porous Media," Jour. Soc. Petroleum Engineers, vol. 246, pp. 412-416, 1969.

[7] Pereze-Rosales, C., and J. J. Martinez, "Structural Characteristics of Granular Porous Media," Jour. Soc. Petroleum Engineers, vol. 252, pp. 364-366, 1971.

[8] Davis, John C., "Optical Processing of Microporous Media," Data Processing in Biology and Geology, J. L. Cutbill (Editor), Academic Press 1970, pp. 69-87.

[9] Preston, F. W., D. W. Green and J. C. Davis, Numerical Characterization of Reservoir Rock Pore Structure, Technical Report, API Project No. 103, University of Kansas Center for Research, Inc., Lawrence, Kansas, August, 1970.

[10] Preston, F. W. and John C. Davis, "Applications of Optical Processors in Geological Images," Machine Perception of Patterns and Pictures, S. E. Fewkes (Editor), National Physical Laboratory, Teddington, England, 1972.

[11] Fara, H. D., and A. E. Scheidegger, "Statistical Geometry of Porous Media," Jour. of Geophy. Res., vol. 66, no. 10, pp. 3279-3284, 1961.

[12] Froberg, C. E., Introduction to Numerical Analysis, Addison-Wesley Publishing Co., p. 63, 1965.

[13] Fukunaga, K., Introduction to Statistical Pattern Recognition, Academic Press, New York, 1972.

[14] Fu, K. S., and J. M. Mendel, Adaptive Learning and Pattern Recognition Systems, Academic Press, New York, 1972.

[15] Miesel, W., Computer Oriented Approaches to Pattern Recognition Systems, Academic Press, New York, 1972.

[16] Nilsson, N. J., Learning Machines, McGraw-Hill, New York, 1965.

[17] Haralick, R. M., and D. E. Anderson, Texture-Tone Study with Application to Digitized Imagery, Technical Report 182-2, University of Kansas Center for Research, Lawrence, Kansas, November, 1971.

[18] Rosenfeld, A. and E. Troy, Visual Texture Analysis, University of Maryland Computer Science Center, Technical Report 70-116, June, 1970.